Check for updates

Fine exploration and green development of ion-adsorption type REE deposits in South China using multi-geophysical technology

Jian-Li Tao[1,2]*, Yi-Chao Deng[1,2], Dong-Xu Ye[1,2],
Bin-Feng Chen[1,2], Yao Zhou[1,2], Jian-Guo Zhong[1,2], Xu Wang[1,2]
and Wei Wang[3]

[1]The Seventh Geological Brigade of Jiangxi Geological Bureau, Ganzhou, China, [2]Key Laboratory of
Ionic Rare Earth Resources and Environment, Ministry of Natural Resources, Ganzhou, China, [3]State
Key Laboratory of Geological Processes and Mineral Resources, School of Earth Sciences, China
University of Geosciences, Wuhan, China

For a long time, the exploitation of ion-adsorption type rare earth (REE) deposits in the southern Jiangxi Province of China have been accompanied by ecological and environmental damage, making the search for green and efficient mining solutions particularly important. Currently, *in-situ* leaching is the main mining technique used for ion-adsorption REE deposits. Before employing this technique, it is imperative to thoroughly investigate the geological mining conditions. Environmental damage caused by the failure to do so, low recovery rates of the original liquor, and secondary geological disasters pose serious challenges to green and efficient mining operations. In this work, microtremor surveying technology was introduced in the Kaizidong mining area in southern Jiangxi Province to refine exploration of the subsurface stratigraphy. By utilizing the wave velocity discontinuity interfaces at 350 m/s and 500 m/s, the layers of the rare earth mine is accurately delineated, including the completely weathered layer, the semi-weathered layer, and the bedrock, providing a critical basis for *in-situ* leaching mining. Subsequently, high-density resistivity method was employed to monitor and measure the flow direction of the original liquor. After the apparent resistivity of the two observational profiles stabilized, they decreased by 57.77% and 63.25%, respectively. Using the variations in resistivity to infer the distribution of the original liquor and simulate its flow direction, the injection and recovery system was adjusted in a timely manner to eliminate potential safety hazards during mining. The exploration of a combined geophysical method of microtremor detection and high-density electrical method has enabled the establishment of a geological model for the entire mine's subsurface structure, guiding the *in-situ* leaching mining process of ion-adsorption REE mines towards an economic, efficient, and green development.

KEYWORDS

ion-adsorption, rare earth mine, *in-situ* leaching, green development, refined exploration

1 Introduction

Rare earth elements, due to their unique atomic structures and excellent physicochemical properties including optical, electronic, and magnetic characteristics, have been globally recognized as critical mineral resources. Particularly, the medium and heavy rare earth elements (MREEs and HREEs) are extensively used in high-technology fields such as aerospace, new energy, semiconductor materials, and medicine, and are thus very expensive and irreplaceable (Wall, 2014; Dushyantha et al., 2020; Zhou et al., 2020; Ji et al., 2021; Cheng et al., 2023). Ion-adsorption REE mines are the primary source of MREEs and HREEs, supplying over 90% of these global resources, underscoring their significance (Moldoveanu and Papangelakis, 2016; Wang et al., 2017; Li and Zhou, 2020). These deposits are characterized by rare earth elements existing in an exchangeable adsorption state as cations within weathered crust, predominantly associated with granitic rocks (Sanematsu and Watanabe, 2016; Costa et al., 2020; Li et al., 2022; Li and Zhou, 2020; Guo et al., 2023). They are widely distributed across seven provinces in Southeast China as well as in countries such as Myanmar, Laos, Malaysia, Philippines, Chile, and Madagascar (Basta et al., 2011; Sanematsu and Watanabe, 2016; Fu et al., 2019; Li et al., 2019; Ram et al., 2019; Borst et al., 2020; Sobri et al., 2023). The ion-adsorption REE mines in the southern Jiangxi region of China are highly valued for mining due to their higher content of MREEs and HREEs, extensive distribution, low radioactivity, and simple extraction processes, making them one of the main economically mined rare earth resources today.

The leaching process for ion-adsorption REE mines has evolved from sodium chloride vat leaching and pool leaching processes, and through continuous improvements, has developed into an *in-situ* leaching process mainly using ammonium sulfate as the leaching agent. This approach ensures that the surface vegetation and the original ecology are preserved during the leaching process (Chen, 2011; Sobri et al., 2024). *In-situ* leaching requires a comprehensive understanding of the geological conditions of the mine, including detailed knowledge of the geology, hydrology, engineering, and environmental geology of the mine. During mining, the layout of the leaching system, including injection wells and collection ditches, is primarily based on surface geological and hydrogeological conditions combined with drilling data, followed by the injection of a large volume of high-concentration leaching solution into the mountain (Xiao et al., 2016). Practice has shown that the distribution characteristics of various strata and other structural fractures in the mines are the main factors affecting the effectiveness of *in-situ* leaching (Moldoveanu and Papangelakis, 2016; Wang L. et al., 2018). Geological heterogeneity and leakage channels make water flow difficult to control and prone to leakage, which not only makes it difficult to ensure recovery rates but also poses a risk of water pollution to groundwater (Zhao et al., 2017; Liu et al., 2022). Additionally, there has been no monitoring of the flow direction of the original liquor during the leaching process, making it impossible to track where the original liquor flows, when it reaches saturation, and whether there are any safety hazards. Therefore, precise detection of the geological structure of the mine and clarification of the flow direction of the leaching agent during mining are crucial for the recovery of the original liquor and rare earth resources (Yaraghi et al., 2019; He et al., 2022). There is an urgent need to develop new technologies and methods to refine exploration and dynamic monitoring of the mining process before mining, to achieve green and efficient development of ion-adsorption REE mines (Luo et al., 2024). During long-term engagement in the exploration and development of rare earths, the use of microtremor detection to accurately determine and divide the stratigraphic sequence of the mine have recently explored in the Kaizidong mining area of southern Jiangxi Province of China. This is complemented by high-density electrical methods to monitor the flow direction of the original liquor, predicting and regulating the seepage of the leaching and recovery process in the mines, thus realizing green and efficient development (Zhong et al., 2022; Chen et al., 2020).

2 Background of regional geology

The Kaizidong mining area is located in Dingnan County, adjacent to Longnan County in the southern Jiangxi region of South China (Figure 1). It is situated within the Cathaysia Block, to the west of the Wuyi uplift, in the middle of the Luoxiao fold belt, spanning across the Wuyi-Luoxiao-Qinhang junction zone. The area is composed of several tectonic units, such as the Yushan and Wuyishan uplift zone as well as the Yingtan-Anyuan, Jiulianshan-Anyuan and Quannan-Xunwu fault zones. Due to complicated geological events, the deep structure in the area is interwoven and complex, with intermittent compression uplifts and tensional fault basins, leading to the formation of NE-NNE trending uplift zones and EW trending tensional magmatic belts in the region. The exposed strata in the region include the Neoproterozoic, Mesozoic, and Cenozoic sequences (Wang W. et al., 2018; Xue et al., 2024). Since the Neoproterozoic, the area successively forms the Neoproterozoic folded basement, Paleozoic sedimentary cover, Mesozoic thrust-fault structural system and fault basins, and Cenozoic loose accumulative sedimentary cover (Xue et al., 2019; Xue et al., 2021; Zhao et al., 2022). Magmatic activity mainly occurred during the Yanshanian and Indosinian periods, mainly comprising monzonitic granite, granodiorite, syenite, granitic porphyry, and granodiorite (Figure 2).

3 Geological background of rare earth elements mineral deposit

The ion-adsorption REE deposits in the southern Jiangxi region area are characterized by wide distribution, abundant reserves, low radioactivity, complete rare earth distribution, and rich content of MREEs and HREEs. Representative deposits include the Kaizidong, Zhongyi and Xunwu deposits, which are enriched in heavy, medium and light rare earth elements, respectively. This work focused mainly on the northern part of the Kaizidong mining area, where the stratigraphy is relatively simple. Quaternary strata are distributed only in the low-lying areas along the valley, with a thickness of 1–3 m, but locally near the mountain foot, it exceeds 3 m. These strata consist of clay and sandy clay. The structural pattern is relatively simple, influenced by fault structure F1, with two main sets of fractures visible. Magmatic rocks are widely exposed, mainly consisting of Early Yanshanian and Late Hercynian granite (Zhao et al., 2014; Zhao et al., 2022; Fan et al., 2023). These two
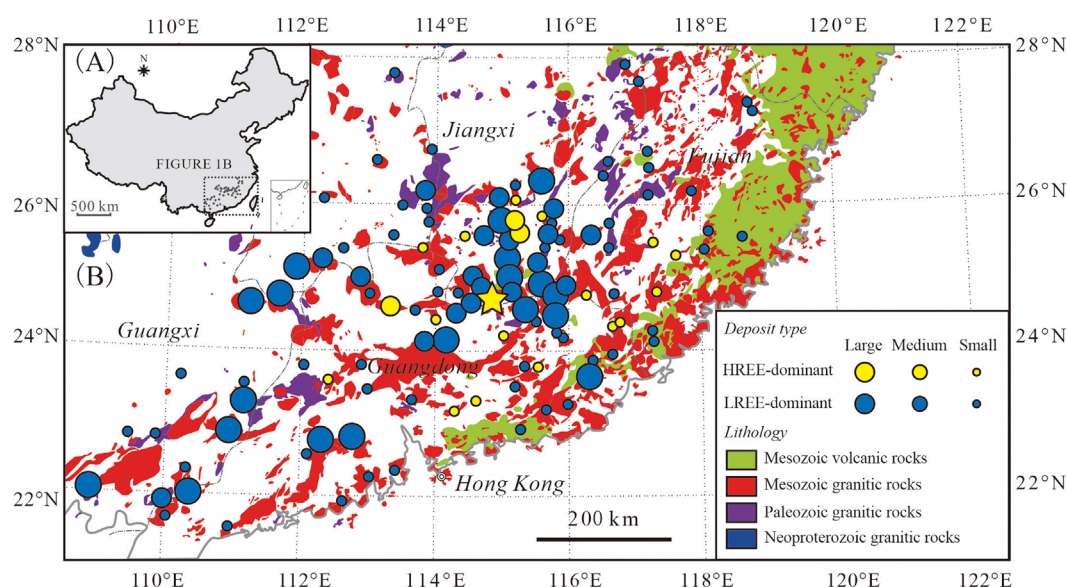
FIGURE 1
(A) The distribution of regolith-hosted REE deposits in South China. **(B)** An enlargement of the box in **(A)** showing the locations of regolith-hosted LREE and HREE deposits and the distribution of granites and volcanic rocks in the region (after Li et al., 2019). The location of the Kaizidong deposit is marked with a yellow star. Note that classification of the HREE-dominant deposits as large, medium, and small is based on rare earth oxide resources of >10,000, 5,000–10,000, and <5,000 t, respectively.
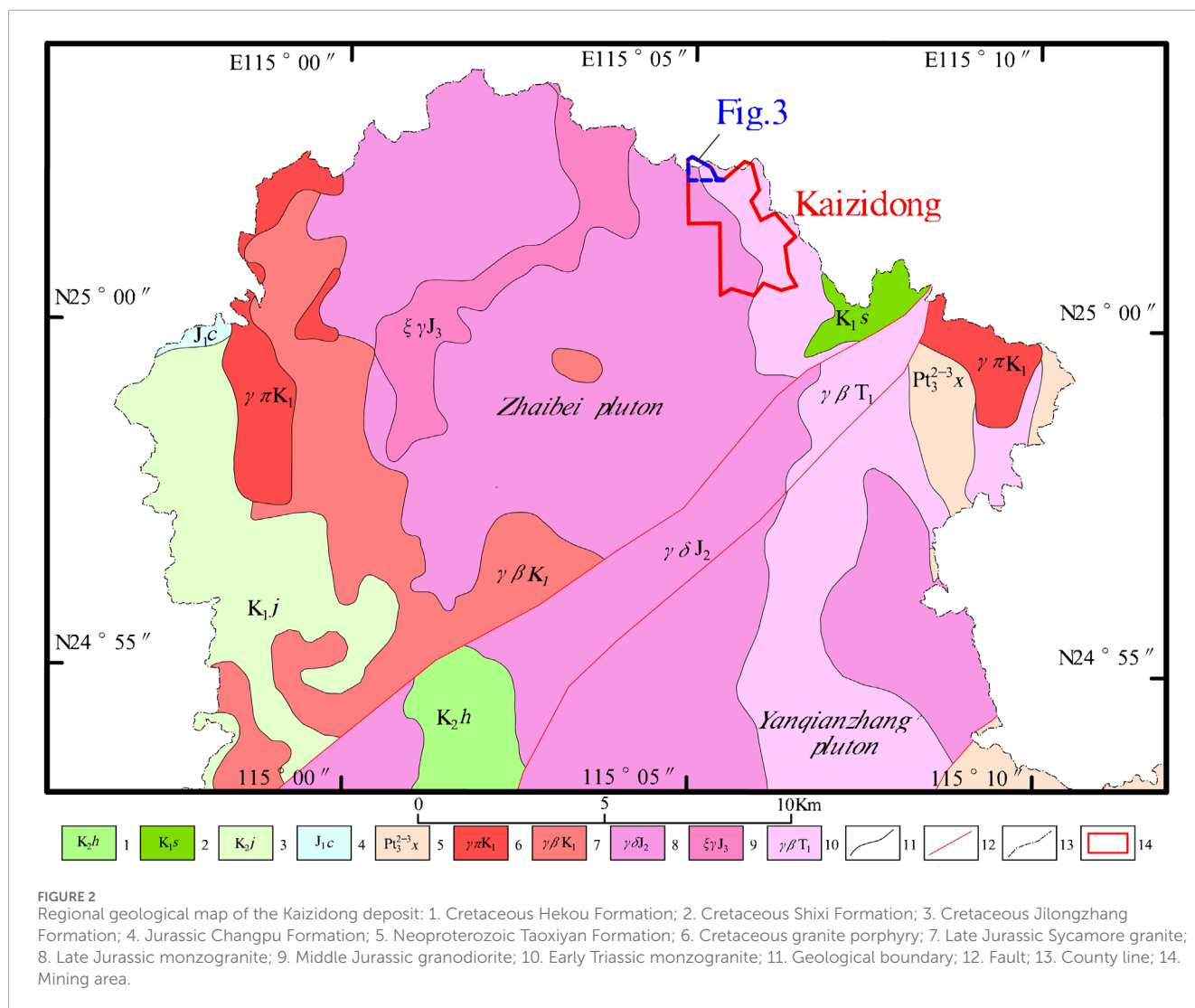
episodes of granite generally extend in a northwest direction, and serve as the parent rocks for ion-adsorption REE deposits within the weathering crust of this area.

The Early Yanshanian granite is characterized by medium-coarse to fine-grained diorite granites, with rocks presenting a light red color and massive structure. The plagioclase and K-feldspar in the rocks are well-formed and euhedral with K-feldspar content reaching 40%–46%. Quartz is anhedral granular and embayed. After weathering, the rocks are mostly brick red, light red or light yellow brown in color, with some parts slightly gray-white. The mineral composition consists of feldspar, quartz, and biotite, while plagioclase and K-feldspar are mostly weathered into earthy, powdery kaolinite-type clay minerals with a slippery feel when handled, and a few K-feldspar crystals still retain their pseudomorphic shapes. Quartz is anhedral granular, with most grain sizes between 2–5 mm, and makes up about 25% of the content. Biotite often exudes iron, displaying a fading phenomenon.

The Late Hercynian rock is characterized by medium to coarse-grained porphyritic and sub-porphyritic biotite-hornblende granites, composed of plagioclase, K-feldspar, quartz, biotite, and muscovite. The phenocrysts are plagioclase and K-feldspar, euhedral to subhedral tabular columnar in shape, with grain sizes of 0.8 × 4.5 cm, and the larger ones can reach 4 × 15 cm. The matrix consists of plagioclase, K-feldspar, quartz, and biotite, with grain sizes between 0.1–0.4 cm. After weathering, the rocks are mostly brick red, light red or light yellow brown, with a loose structure. The plagioclase and K-feldspar have largely weathered into earthy, powdery kaolinite-type clay minerals with a slippery feel when handled, with K-feldspar often retaining its crystal pseudomorphs. Quartz appears as anhedral granular, with most grain sizes less than

3 mm, accounting for about 20%–25%. Biotite often exudes iron, showing a fading phenomenon, and muscovite is fine flaky.

The orebody is mainly hosted within the completed weathered layer of granite, distributed in a pseudo-stratiform manner throughout this layer. The planar shape is controlled by the morphology of the weathering crust, extending from the mountain top in a northeast direction along two main ridges to the southeast. On the surface, the orebody is comb-shaped, with its morphology and occurrence generally consistent with the topographic changes. The profile shape of the orebody is relatively simple, overall cap-shaped, sloping from the mountain top outward, with a dip angle along the ridge of generally 5°–10°, and a slope angle on the sides of about 20°–25°. Most parts of the orebody are covered by saprolite or soil layers, with an average thickness of 1.03 m. The thickness of the orebody varies with the topographic position and is closely related to the micro-geomorphological location, generally thicker at the mountaintop, followed by the ridge, and thinner on the slopes and at the foot of the slopes. The coefficient of variation in thickness is 73.79%, indicating relatively stable thickness. The original rock structures and textures are mainly preserved, while strong weathering leads to the destruction of the original rock structures and textures. The main ore structures and textures include: sandy clay texture, spotted structure, loose earthy structure, and massive structure. The ore has a relatively coarse grain size, with quartz particle sizes ranging from 2 to 8 mm. The main mineral components of the completed weathered layer are: clay minerals (30%–40%), quartz (25%–35%), feldspar (20%–40%), and mica (5%–10%), with kaolinite-type clay minerals, quartz, and K-feldspar together accounting for about 95%, followed by magnetite and biotite making up about 5%, and minor amount of resistant rare earth minerals and accessory minerals.

FIGURE 2
Regional geological map of the Kaizidong deposit: 1. Cretaceous Hekou Formation; 2. Cretaceous Shixi Formation; 3. Cretaceous Jilongzhang Formation; 4. Jurassic Changpu Formation; 5. Neoproterozoic Taoxiyan Formation; 6. Cretaceous granite porphyry; 7. Late Jurassic Sycamore granite; 8. Late Jurassic monzogranite; 9. Middle Jurassic granodiorite; 10. Early Triassic monzogranite; 11. Geological boundary; 12. Fault; 13. County line; 14. Mining area.

4 Microtremor detection for stratigraphic division of ion-adsorbed rare earth mines

4.1 Application of microtremor detection

Microtremor exploration is based on the theory of steady random processes (Anikiev et al., 2023). It extracts Rayleigh wave phase velocity dispersion curves from the microtremor signals recorded by arrays. By inverting these dispersion curves, the subsurface medium's S-wave velocity structure can be obtained. In rare earth mines, the variable degree of weathering or the presence of structural fractures can cause changes in wave propagation velocity. By understanding the variation patterns of subsurface medium wave velocity, it is possible to infer the distribution characteristics of the subsurface space, with the aim of detecting the underground spatial structure of rare earth mines (Simiyu, 2009; Jia et al., 2022). It is generally believed that the wave velocity of each layer in a mine should increase progressively from top to bottom. The wave velocity of the weathered profile

is directly related to the degree of weathering with loose soil layer and the completed weathered layer having the lowest and the bedrock having the highest value. Therefore, the interfaces of sudden wave velocity changes can be used for the division of different strata.

By utilizing the microtremor detection method, faint vibrations from the mine's subsurface space are collected, and the dispersion curves of surface waves are extracted from the microtremor signals. By inverting these dispersion curves, the transverse wave velocity structure of the subsurface medium is obtained, which can then be used to infer the depth and thickness of the different layers in the mine (Ibs-von Seht and Wohlenberg, 1999; Sun et al., 2009; Wang Z. W. et al., 2018). This technique allows for the economical, efficient, and environmentally friendly accurate delineation of the various strata within a rare earth mine, determining the thickness of the weathered crust ore body and the bedrock floor for *in situ* leaching (Ibs-von Seht and Wohlenberg, 1999; Wang Z. W. et al., 2018). By establishing a geological model of the entire mine's underground structure, it provides a crucial basis for mine exploration and *in situ* leach mining operations.

4.2 Profiles microtremor detection

This work takes the Kaizidong ion-adsorbed REE mine in the southern Jiangxi as an example. Microtremor detection is conducted to divide the strata of the rare earth mine, and it is combined with the drilling data of the mining area for comparison to verify the accuracy of this method.

Figure 3 shows the layout of the microtremor detection profiles. There are five profiles, all perpendicular to the main ore body within the measured area. The orientation of the profiles is 32°, with a spacing of 40 m between them. The length of profiles PM01 and PM05 is 160 m, while profiles PM02, PM03, and PM04 are 280 m long. The observation points on all profiles are spaced at intervals of 5 m.

4.3 Workflow of microtremor detection

For this survey, the TVG-63H three-component nodal seismometer is used for observation. This instrument is a new generation of intelligent nodal seismometers that integrates a high-sensitivity seismic sensor, a high-performance collector, satellite and crystal oscillator for high-precision timing, intelligent anti-theft and status monitoring, a 4G/5G Internet of Things remote communication module, a high-capacity lithium battery, and charge-discharge control (Yang and Guo, 2020). Due to the complex terrain, a linear array is used for observation. The array is laid out along the direction of the survey line. Real-Time Kinematic (RTK) is used to mark the predetermined measurement points accurately. Pits are dug at these points for the burial of instruments. During burial, the level bubble of the instrument should be centered. After leveling the ground with a shovel, the TVG-63H three-component nodal seismometer is placed horizontally on the measurement point. Once the instrument is in place, the devices at each station are turned on, personnel clear the area, and after the instrument enters its normal working state, the start time of the synchronous data collection by each instrument is recorded. In addition to recording the start time of data collection, it is necessary to log the instrument number corresponding to each measurement point in the record sheet, as well as information about human disturbances, terrain features, and geological summaries at the measurement point for reference during data processing (Chen et al., 2018). After an effective observation duration of 1 hour, the instruments are turned off and moved to the next measurement point.

5 High-density electrical resistivity monitoring of original leach solution flow

5.1 Monitoring for the flow of original solution

As previously mentioned, microtremor detection can be used to delineate the layered structural conditions of a mine, thereby guiding the layout of the *in-situ* leachate injection and recovery system (Ghosh and Sivakumar, 2018; Wang Z. W. et al., 2018). However, during the *in-situ* leaching process, there is a lack of tracking for the

flow direction of the original leach solution. Because of the complex geological conditions of mines, the flow direction of the original solution can be unclear, and the amount of recovery solution is often unpredictable and highly variable, dependent on the weather condition (He et al., 2022; Traore et al., 2023). High-density electrical resistivity is extremely sensitive to changes in electrical resistance. The leaching solution can alter the electrical resistivity of the strata during the permeation process through the mine. The electrical resistivity is typically lower in strata with higher water content, while bedrock and sections with poor permeability generally have higher resistivity or minor changes (Bharti et al., 2021).

Therefore, after the injection of the leach solution, high-density electrical resistivity measurements can be conducted at regular time intervals on each profile. This results in a series of time-correlated resistivity cross-sections for each profile, which can be used to approximate a dynamic simulation of the flow direction of the original solution.

5.2 Monitoring layout for original solution flow direction

The high-density electrical resistivity method is also used to monitor the flow direction of the original solution in the aforementioned mine, and the results are validated and explained in conjunction with the actual outflow situation. Two high-density monitoring profiles are arranged in the demonstration mine block, where: Profile PM01 has 50 points with a point spacing of 4 m, giving a total profile length of 200 m, and the profile direction is A-B. Profile PM02 has 60 points with a point spacing of 4 m, resulting in a total profile length of 240 m, and the profile direction is C-D.

In order to facilitate the explanation and verification, the various types of injection and recovery systems for this mine are also roughly indicated in the schematic diagram (Figure 4). It can be seen that both monitoring profiles traverse the injection range of this mine block. The ridge serves as the boundary line, with no injection carried out in the eastern part and no recovery projects arranged. The recovery pool is located in the southwestern part of the mine block, and a collection ditch is arranged along the foothills on the western side of the mine block, with the majority of horizontal drilling distributed along the collection ditch. It should be noted that the horizontal drill numbers 1 to 5 in the diagram are only indicative of their approximate locations and are not representative of the quantity. The lengths of the tunnels and horizontal drills are also not their actual extension depths but only indicate their general extension directions.

5.3 Monitoring process for original solution flow direction

This monitoring period extended from May 23 to 2 August 2023, with a total of 68 days of leachate injection and 54 days of monitoring. Detailed records were kept daily, including the weather conditions, rainfall, volume of injected leachate, number of injection wells, and the precipitation of original solution (Table 1). The first emergence of original solution was observed in recovery tunnel No. 1 on July 12, followed by the emergence at horizontal drill No. 3 on
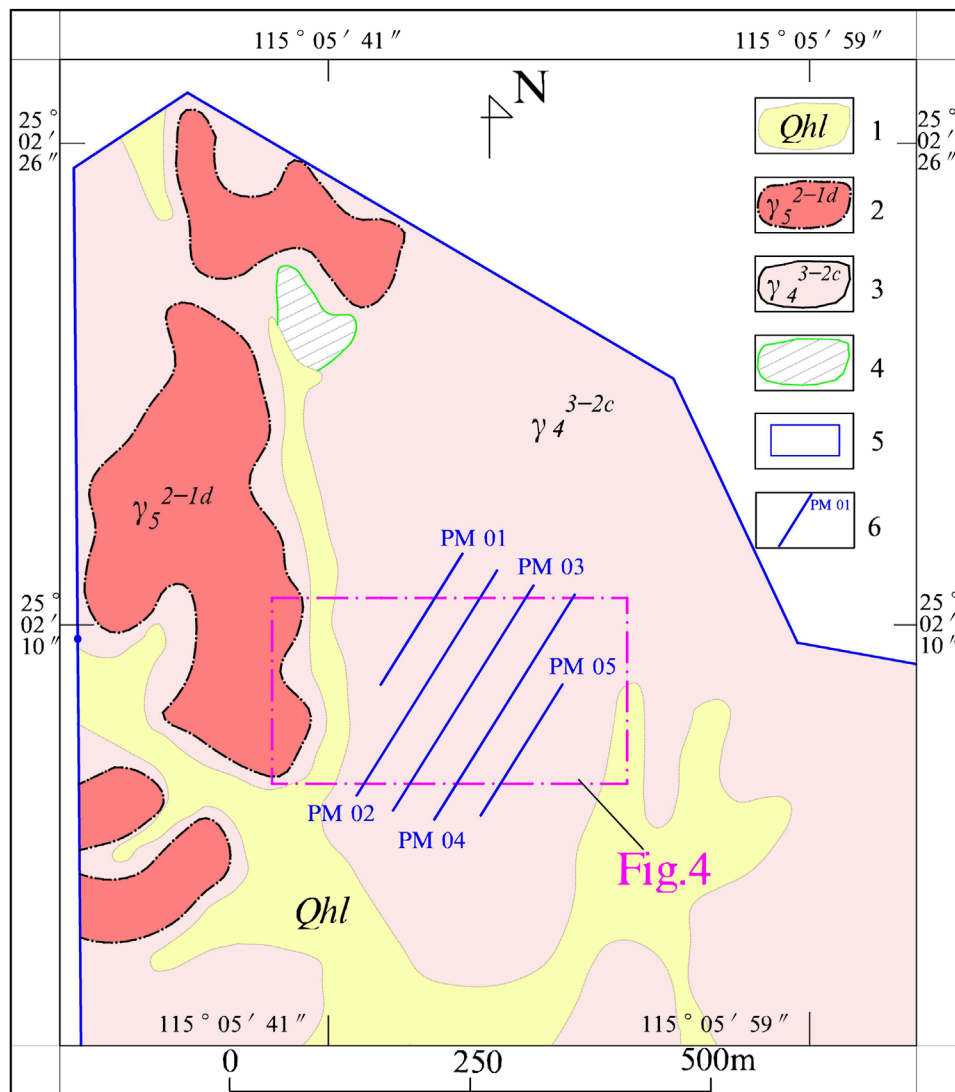
FIGURE 3
Simplified Geological Map of the Northern Area of the Kaizidong Mining District. 1. The Quaternary Lianxu Formation including clay, sandy clay and gravel layer from base upwards; 2. Early Yanshanian medium-fine-grained biotite granite; 3. Late Hercynian medium-coarse grain porphyry monzonitic granite; 4. Bedrock area; 5. Mining area; 6. Layout diagram of microtremor detection.

July 20. Subsequently, original solution was also detected emerging from horizontal drill No. 4 and recovery tunnel No. 2. The last location to show the emergence of original solution was horizontal drill No. 2. No original solution emerged from the other recovery locations throughout the entire monitoring period.

After continuous rainfall from July 16th to 20 July 2023, the decrease rate apparent resistivity for PM01 increased, while no such phenomenon was observed for PM02 (Table 1). This difference is likely resulted from the locations of the two profiles (Figure 4). For the PM02 that passes through hillside, the rainfall flows into the gully along the surface of the hillside, having no significant impact on the original fluid flow direction and the overall apparent resistivity changes in the survey area. However, when PM01 passes through the top of a hill, some of the rainfall infiltrates into the ground through the injection holes, accelerating the rate of apparent

resistivity decrease in the survey area, but with no significant impact on the original fluid flow direction. In the later stages of fluid injection, the apparent resistivity values of the two profiles tended to converge, indicating that under certain conditions, continuous rainfall will accelerate the rate at which the original fluid infiltrates into the stratum, but has no significant impact on the fluid flow direction.

After the monitoring was completed, outliers were removed before using 2D high-density resistivity imaging software for format conversions. Subsequently, the elevations of the measurement points were added using Surfer16 and data inversion was carried out with Res2dinv. Finally, mapping was accomplished using Mapgis6.7 and Surfer16. Based on the variations in apparent resistivity observed in the two profiles after mapping,it was observed that as the leachate injection into the target mining block progressed, the
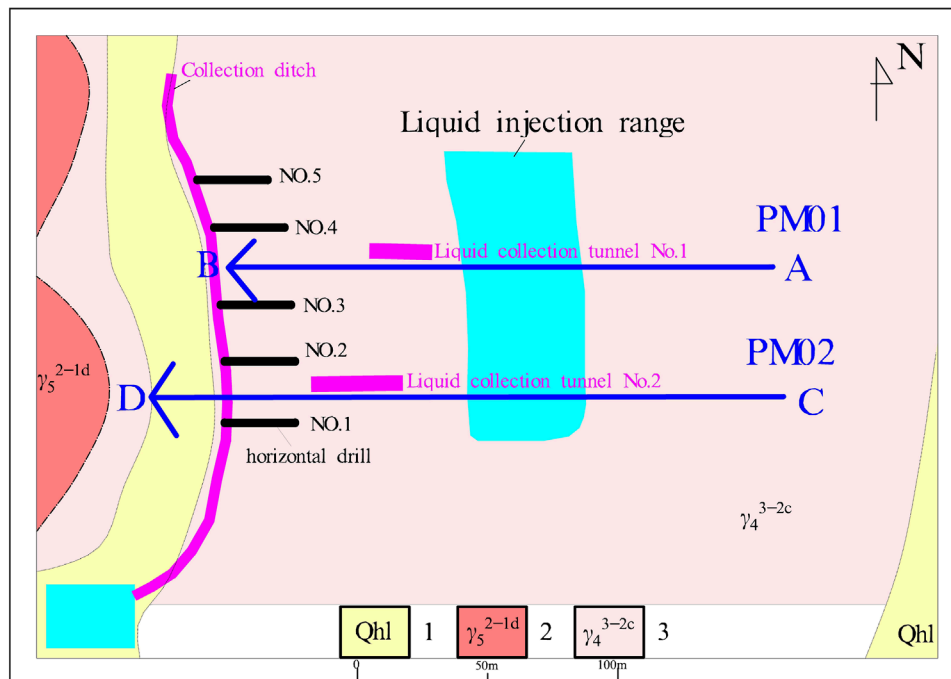
FIGURE 4
Schematic diagram of reacted liquor monitoring work. The Quaternary Lianwei Formation with clay and sandy clay in the upper part and gravel layer in the lower part; 2. Early Yanshanian medium-fine grained biotite granite; 3. Late Variscan medium-coarse grained porphyroid two-mica monzonitic granite.

overall apparent resistivity of the block showed a downward trend. For profile PM01, the resistivity stabilized relatively on July 11, with the average apparent resistivity decreasing from the initial 989.05 Ω-meters to 383.86 Ω-meters, a total reduction of 57.77%. For profile PM02, the resistivity tended to stabilize relatively on July 25, with the average apparent resistivity decreasing from 983.46 Ω-meters to 361.38 Ω-meters, a total reduction of 63.25%. This intuitively reflects the impact of the leaching solution injected into the strata on the resistivity and also represents the saturation of the original solution in the formation (Figure 5).

6 Discussion

6.1 Microtremor survey inference and verification

After the data collection was completed, various processing was carried out on the data, and the Surface Plus—advanced version software for surface waves was used to create subsurface shear wave velocity profiles. These profiles are used to infer the conditions of the underground space. From the inverted section diagram (Figure 6), it is clearly observed that there are two interfaces where the wave velocity changes abruptly within the mine's underground space, located at 350 m/s and 500 m/s, respectively.

Based on the pattern of wave velocity changes, areas with shear wave velocities less than 350 m/s (shown in blue on the map) are delineated as the completely weathered crust. For the layer below, where the velocities range from 350 to 500 m/s (shown in light blue

transitional area), it is inferred to be the semi-weathered crust. The area further down, where the wave velocity exceeds 500 m/s (shown in the red area), is deduced to be the bedrock.

To validate the accuracy of the microtremor inferred interfaces, drilling data from the 'Gannan' drills (a manual drill that can perforate through the completely weathered layer and into the semi-weathered layer for more than 0.5–1 m) were collected and overlaid for comparison on each profile. There were a total of 15 'Gannan' drills located on these profiles, and it was found that the depths drilled by the vast majority of these drills matched the completely weathered crust interface as inferred in this study. The only exception was the GNZ2256 drill hole on the PM04 profile, which showed a slight deviation from the inferred interface. Since 'Gannan' drilling can only reveal the completed weathered layer, mechanical drills ZK001 and ZK002 were carried out on profiles PM02 and PM04, respectively, to verify the accuracy of the inferred Semi-weathered layer and bedrock. In the diagram, the mechanical drill indications in light grey, dark grey and black represent the thickness of the exposed completed weathered, semi-weathered and bedrock layers, respectively. It can be seen that the layers exposed by the ZK001 mechanical drill on the PM02 profile match the inferred interfaces well, while the layers exposed by the ZK002 mechanical drill on the PM04 profile show a slight deviation. Additionally, the depth of the completed weathered layer exposed by ZK002 is deeper than the depth drilled by the 'Gannan' drill, which may be primarily due to the disturbance of the original rock structure during mechanical drilling, resulting in the exposed layers being slightly deeper than the actual layers.

TABLE 1 Diary monitoring of reacted liquor.

Date	Number of monitoring points	Weather	Rainfall amount	Number of injection wells	Volume of injected leachate (m^3)	Outflow condition
2023/5/23	110	Overcast	0	0	0	—
2023/5/24	110	Overcast	0	300	300	No Outflow
2023/5/25−2023/7/10 ellipsis						
2023/7/11	110	Clear	0	300	300	No Outflow
2023/7/12	110	Clear	0	300	300	Recovery Tunnel No.1
2023/7/13	110	Clear	0	400	320	Recovery Tunnel No.1
2023/7/14	110	Clear	0	400	320	Recovery Tunnel No.1
2023/7/16	110	Thunder shower	10	400	320	Recovery Tunnel No.1
2023/7/17	110	Thunder shower	10	400	320	Recovery Tunnel No.1
2023/7/19	110	Thunder shower	5	400	320	Recovery Tunnel No.1
2023/7/20	110	Thunder shower	5	400	320	Recovery Tunnel No.1, Horizontal Drill 3
2023/7/21	110	Cloudy	0	400	320	Recovery Tunnel No.1, Horizontal Drill 3
2023/7/22	110	cloudy	0	400	320	Recovery Tunnel No.1, Horizontal Drill 3
2023/7/25	110	Thunder shower	5	400	320	Recovery Tunnel No.1, Horizontal Drill 3, Horizontal Drill 4
2023/7/26	110	Cloudy	0	400	320	Recovery Tunnel No.1, Horizontal Drill 3, Horizontal Drill 4, Recovery Tunnel No.2
2023/7/27	110	Cloudy	0	400	320	Recovery Tunnel No.1, Horizontal Drill 3, Horizontal Drill 4, Recovery Tunnel No.2
2023/7/28	110	Cloudy	0	400	320	Recovery Tunnel No.1, Horizontal Drill 3, Horizontal Drill 4, Recovery Tunnel No.2, Horizontal Drill2
2023/7/29	110	Cloudy	0	400	320	Recovery Tunnel No.1, Horizontal Drill 3, Horizontal Drill 4, Recovery Tunnel No.2, Horizontal Drill 2
2023/7/30	110	Cloudy	0	400	320	Recovery Tunnel No.1, Horizontal Drill 3, Horizontal Drill 4, Recovery Tunnel No.2, Horizontal Drill 2

TABLE 1 (*Continued*) Diary monitoring of reacted liquor.

Date	Number of monitoring points	Weather	Rainfall amount	Number of injection wells	Volume of injected leachate (m^3)	Outflow condition
2023/7/31	110	Cloudy	0	400	320	Recovery Tunnel No.1, Horizontal Drill3,Horizontal Drill4, Recovery Tunnel No.2, Horizontal Drill 2
2023/8/2	110	Cloudy	0	400	320	Recovery Tunnel No.1, Horizontal Drill3,Horizontal Drill4, Recovery Tunnel No.2, Horizontal Drill 2

FIGURE 5
Change in Resistivity of reacted liquor Monitoring.
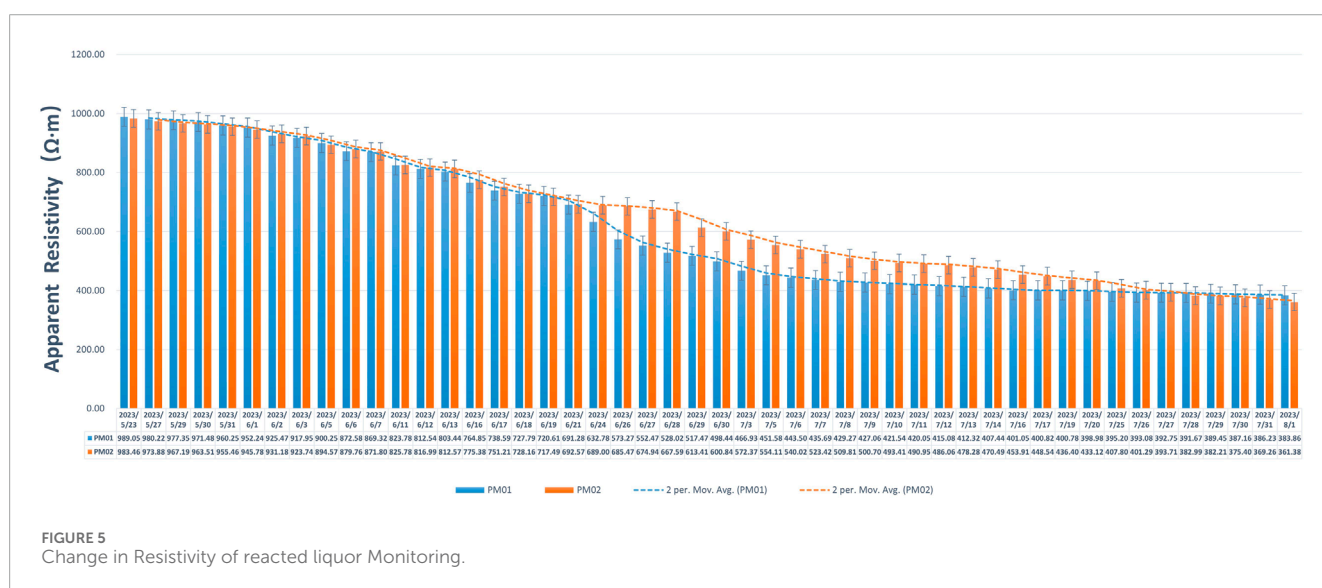
Through this validation, it is known that the microtremor inferred stratification interfaces are consistent with the 'Gannan' drilling data, and the overall structure of the survey area is relatively stable. Microtremor detection technology can accurately delineate the different weathered layers within a rare earth mine. This method is economical, efficient, and green, and it contributes to establishing a geological model of the entire mine's underground structure (Ibs-von Seht and Wohlenberg, 1999; Wang Z. W. et al., 2018). This provides a critical basis for mine exploration and *in-situ* leaching mining, supporting the detailed detection and *in-situ* leaching mining of ion-adsorption REE mines.

6.2 Original liquor flow monitoring results and verification

In this mining area, a total of 54 observations were conducted on each of the two profiles, with each observation showing varying degrees of change, and these changes were largely linear. Here, we will not list each observation but will select the monitoring results from the first day of liquid injection (23 May 2023), the gradual emergence of original liquor (12 July 2023), and the late stage of liquid injection (2 August 2023) for analysis and verification. To facilitate a clear and comparative analysis, the resistivity color scale of all profiles has been standardized, using a blue-to-red transition to represent the change in the stratum's resistivity from low to high.

This is the inversion profile of the original liquor monitoring for PM01 (Figure 7). It is apparent that at the initial stage of liquid injection, the stratum resistivity is predominantly in large areas of red, indicating an overall higher resistivity value, which suggests that the subsurface space is relatively dry. From this profile on July 12, as the injection of liquid continues, the original liquor further penetrates, and the apparent resistivity significantly decreases. The low-resistance areas mainly extend from the ridge to both sides, concentrated around the 64–160 m section of the profile, with apparent resistivity values less than 100 Ω m. Continuing the injection until 2 August 2023, the apparent resistivity of the mining block substantially reduces, with the low resistance mainly extending towards the end B, indicating that most of the original liquor has penetrated towards the end B (Figure 7). However, a large low-resistance area also appears at the end A, suggesting that some of the original liquor may seep towards the east side. After the resistivity stabilizes, the large low-resistance area on the
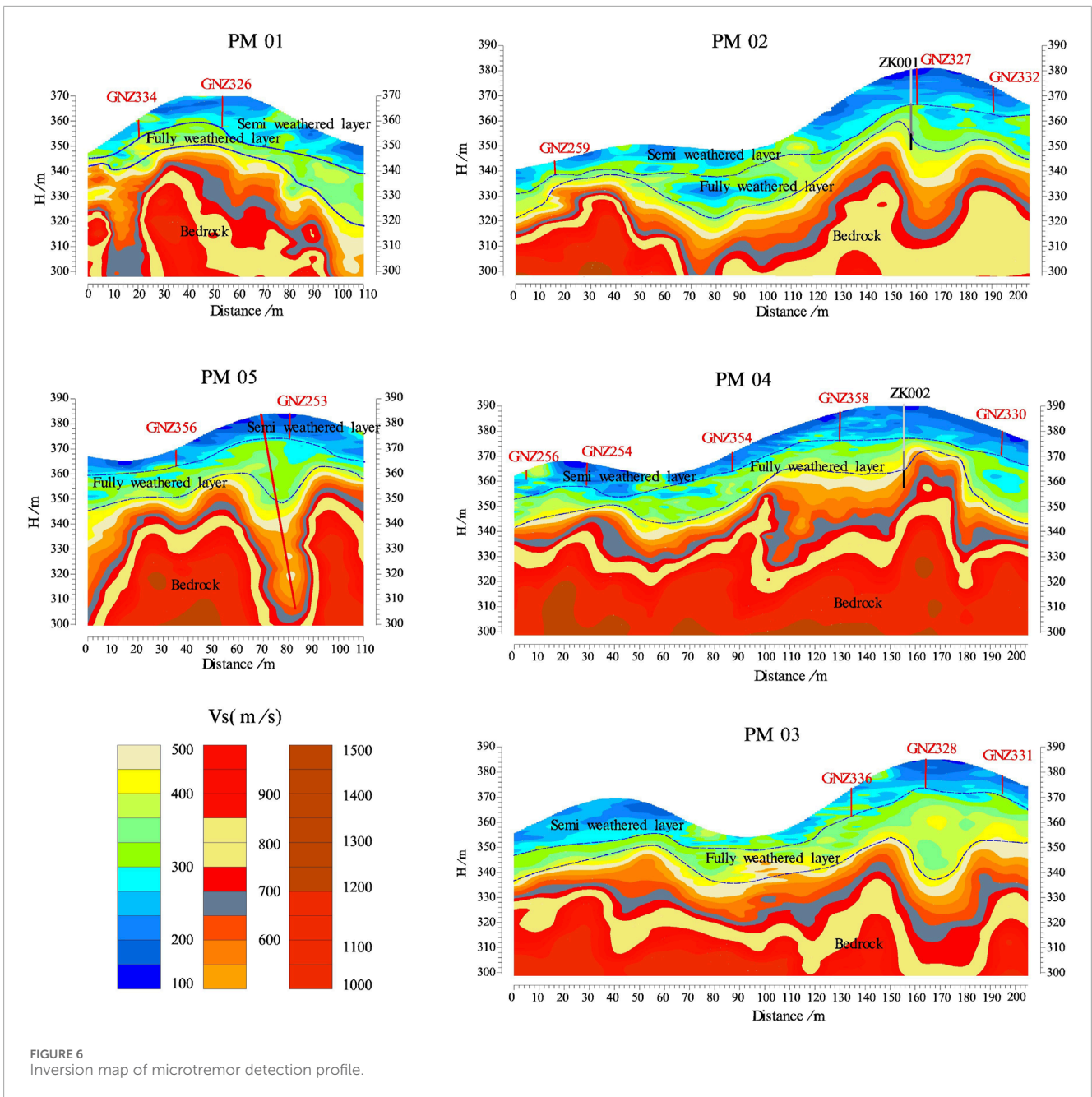
FIGURE 6
Inversion map of microtremor detection profile.

side B of the profile suggests that horizontal drills 3, 4, 5, and the No. 1 liquid collection tunnel could all have original liquor emerging. The low-resistance area at 64–88 m extending towards the side A suggests that the side A may also have original liquor emerging. Notably, near 128 m on the profile, the blue low-resistance area has extended to the surface, indicating that the original liquor in this section may be oversaturated, with the risk of spilling out along the injection hole and the potential for landslides.

Upon field verification (Figure 8), the monitoring inference results are essentially consistent with the actual situation, with original liquor emerging from horizontal drills 3, 4, and the No. 1 liquid collection tunnel. The injection hole near 128 m on the profile also clearly shows the original liquor near the surface, and the injection personnel have also promptly limited the flow based on the

observation results to prevent the original liquor from flowing along the surface and to control risks. It is worth mentioning that after we stopped observations, on August 7, original liquor also emerged on the A-side slope, consistent with the observation inference results.

Analyzing the inversion section of the PM02 profile (Figure 9), when the liquid injection just started, the apparent resistivity of the underground space was mainly high resistance. On July 12, the range of the low-resistance area expanded, extending towards the side D. From the monitoring results on August 2, the apparent resistivity of the mining block continued to decline, the low-resistance area expanded, and tended to stabilize. Similar to the PM01 profile, the surface apparent resistivity values in the 80–144 m section of the profile were very low. Field surveys revealed that the liquid in the injection holes was clearly visible, indicating that the injection volume in this

FIGURE 7
Cross section of PM01 reacted liquor monitoring inversion.
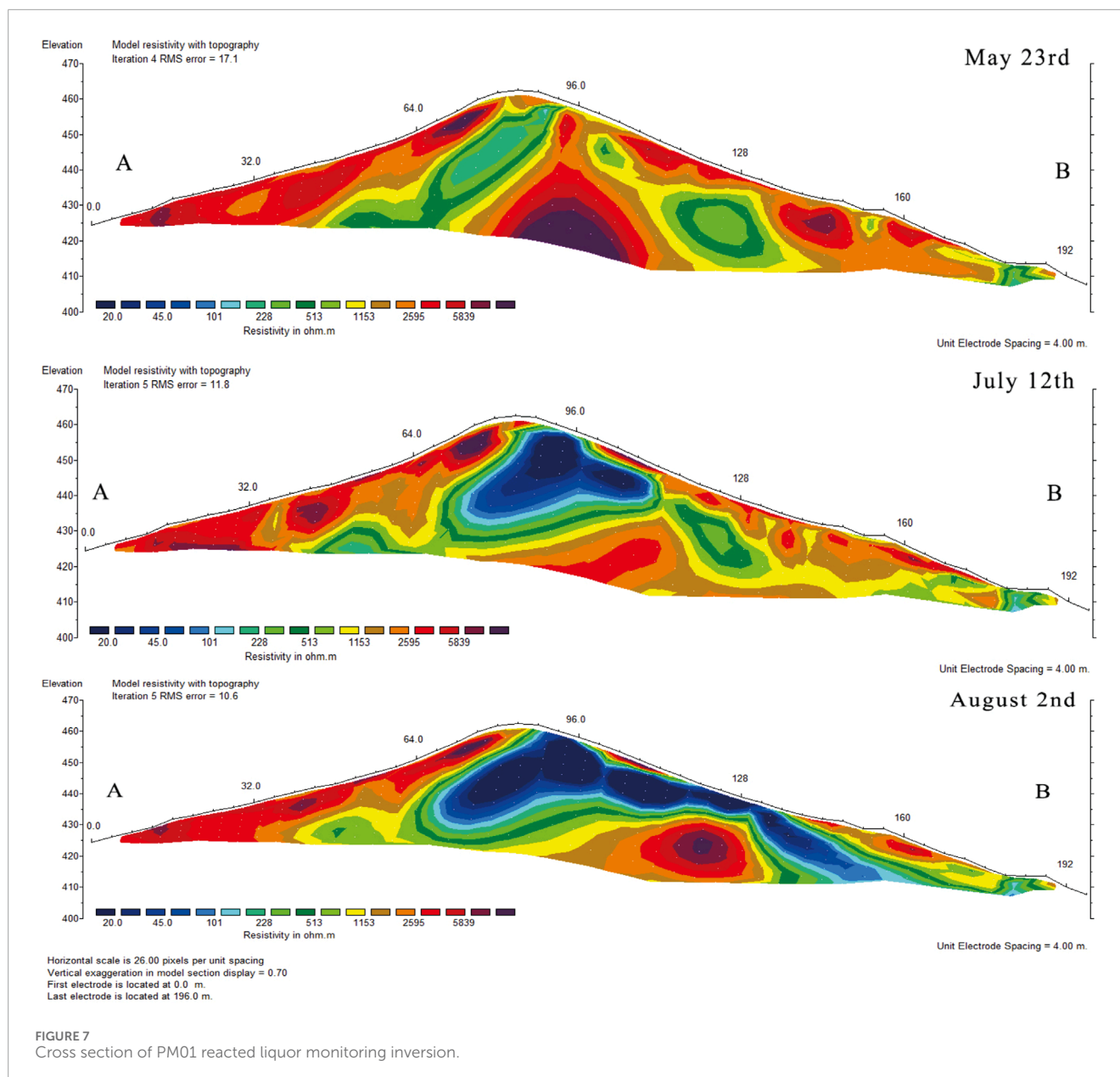
area had reached saturation, and the injection personnel also promptly limited the flow to prevent risks. Similar to PM01, there were signs of leakage towards the side C below the low-resistance area. Combining the results of PM01, it is highly probable that the original liquor could emerge from the eastern slope or the foot of the mountain. It is also advisable for the mine to pay attention to the injection-recovery ratio and to promptly check at the foot of the eastern side of the mining block to see if any original liquor has emerged.

Based on the above analysis, it can be determined that the liquid collection conditions for PM02 are good, and the emergence of the liquid should mainly be concentrated at the No. 2 liquid collection tunnel. The horizontal drills 1 and 2, which are positioned lower, show higher resistivity values, suggesting that the liquid emergence there should be average. However, it is inferred that the eastern side of the ridge may actually experience some original liquor seepage.

Upon field verification, as detailed in (Figure 8), the amount of liquid emerging from the No. 2 liquid collection tunnel is substantial, while the liquid output from horizontal drill 2 below is average. At the location of horizontal drill 1, there has been no emergence of original liquor from beginning to end, and there has been some seepage of original liquor on the eastern slope in the later stages, which is consistent with the predicted results.

In the *in-situ* leach mining process, high-density electrical resistivity measurements enable the creation of apparent resistivity cross-sections for each profile (Bustillo Revuelta, 2018). These cross-sections allow for the inference of the distribution state of the original liquor. By observing the variations in apparent resistivity over time, the permeation process of the original liquor can be inferred, which allows for the simulation of the original liquor's flow direction. Timely optimization and adjustment of the injection and

FIGURE 8
Liquid collection system of PM 01 and PM 02. **(A)** the location of horizontal drill No. 1; **(B)** liquid collection from horizontal drill No. 4; **(C)** liquid discharge of horizontal dirll NO. 3; **(D)** the location of surface injection hole; **(E)** liquid collection tunnel with recovery status; **(F)** collection tunnel with recovery status of liquid from horizontal drill No. 2.

recovery system can be carried out based on these observations, eliminating potential safety risks during the mining process.

6.3 The combination of detailed exploration and green development

Ion-adsorption rare earth mines have successively undergone three different leaching methods: pool leaching, heap leaching, and *in-situ* leaching. At present, *in-situ* leaching is widely used, and the extraction process is continuously advancing towards greener methods (Yang et al., 2013; Moldoveanu and Papangelakis, 2016; Sanematsu and Watanabe, 2016; Liu et al., 2019). Both pool leaching and heap leaching require the mining and stripping of ore bodies, that is, transferring the ion-adsorption rare earth mines to leaching pools through mechanical excavation, which is a typical "mountain-moving" operation and causes severe damage to vegetation (Azizi et al., 2022; Meng et al., 2023). Due to the high cost of mechanical excavation,

FIGURE 9
Cross section of PM02 reacted liquor monitoring inversion.
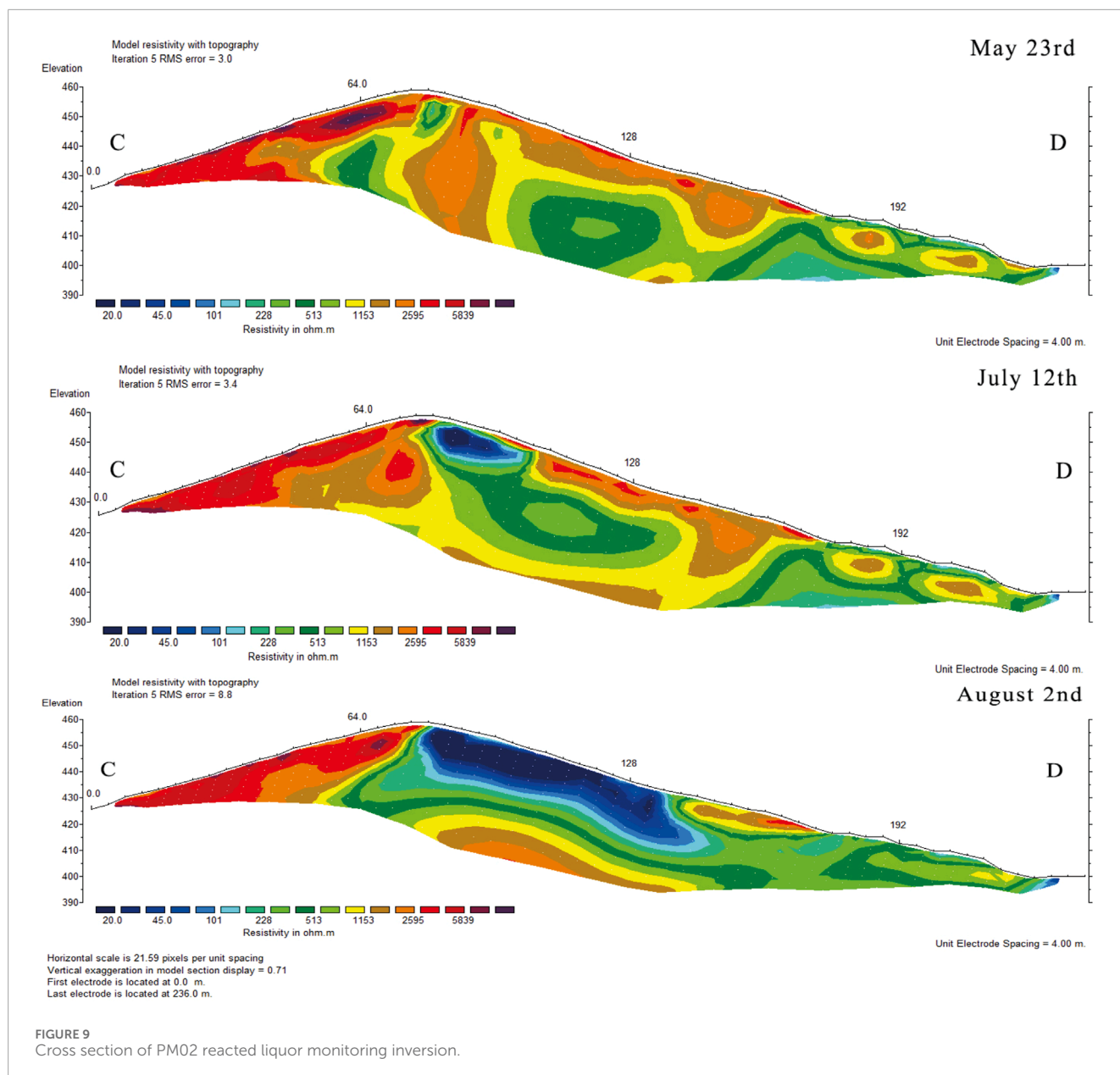
leaching usually starts with ore bodies that are of high grade and easier to strip, following the practice of "mining the rich and abandoning the poor" or "mining the easy and abandoning the difficult," resulting in significant resource wastage (Asadollahzadeh et al., 2021; Chen et al., 2022). Since most low-grade and difficult-to-mine ore bodies are not developed, the utilization rate of rare earth resources is only 30%–40%. *In-situ* leaching does not require mountain excavation, only drilling and injecting fluids in place, which causes less impact on the ecological environment. However, because of the diversity of geological conditions, the production technology is more challenging (Kanazawa and Kamitani, 2006; Chi and Liu, 2019; Dushyantha et al., 2020), especially for ore bodies with complex geological structures, such as rare earth mines without a bedrock bottom, where leachate leakage is severe, and the recovery of leaching original liquor is difficult. This significantly reduces the recovery rate of rare earth, generally to 50%, and is accompanied by a low recycling rate of associated resources,

secondary resources, and chemical materials (Costis et al., 2021). The current situation of low resource utilization limits the expansion of the ion-adsorption rare earth development field and also restricts the rapid transformation and upgrading of the rare earth industry (Tian et al., 2010; Guo et al., 2018; Guo et al., 2019; Chen et al., 2022).

To achieve efficient and green development of ion-adsorption rare earth mines, it is necessary to conduct refined exploration of the mines to understand the geological structure, as well as to monitor the original liquor accurately and effectively during the mining process (Chen et al., 2022). For example, before *in-situ* leaching mining of each rare earth mine, refined exploration can be carried out using microtremor detection methods to collect weak vibrations from the underground space of the mine (Smith et al., 2013). By extracting the dispersion curves of surface waves from microtremor signals and inverting these curves, the shear wave velocity structure of the underground medium can be obtained. Using this velocity

structure in combination with borehole data, an underground space layer wave velocity model can be established (Wang Z. W. et al., 2018). This model allows for economical, efficient, and green accurate delineation of the various strata of the rare earth mine, determining where the bottom of the mine is located, whether there are any fracture zones, the presence of groundwater, and whether there are any leakage channels, among other conditions (Ibs-von Seht and Wohlenberg, 1999; Balaram, 2019; Li et al., 2020).

After comparing the real geological conditions of the ore body revealed by drilling (both 'Gannan' drilling and mechanical drilling) with the inversion results of the microtremor survey profile, it was found that the thickness, geological interfaces, and fault structures of ore body displayed by both methods are basically consistent (Figure 6). This indicates that this model is able to provide real geological conditions of ore body. It also enables the mining fluid system's layout to be targeted effectively. During the mining process, high-density resistivity methods are used for real-time measurements to effectively monitor and track the entire *in-situ* leaching process by observing the changes in the resistivity of the underground space as the leaching fluid permeates and flows (Sinclair and Thompson, 2015). This improves the efficiency of the injection and recovery of the fluid and reduces the safety hazards during the mining process. It is important to note that the high-density electrical method, with its advantages of sensitivity to resistivity changes, ease of cabling, and convenience in data acquisition, is suitable for monitoring the flow direction of original liquor in rare earth mines. Meanwhile, microtremor exploration is also applied in stratigraphic division within rare earth mines due to its advantages of not requiring artificial seismic sources, strong exploration capabilities, and high efficiency. However, factors such as complex signal processing and noise filtering for both methods need to be considered and addressed in practical applications. The close and effective coordination of these two methods can lead to highly constructive innovations in the mining of ion-adsorption mines.

7 Conclusion

Microtremor detection technology can detail the interface of different weathering degrees of ion-adsorption rare earth and identify the shape of the impermeable bottom plate and concealed underground fractures. This aids in the refined exploration of rare earth mines, provides a geological basis for the precise layout of mining projects, and improves the recovery rate of leaching original liquor.

High-density resistivity method can intuitively perceive the flow and distribution of the original liquor, turning the black box operation of original liquor recovery into visualization. This allows for targeted optimization and adjustment of the injection and recovery system, timely elimination of safety hazards, and provides technical support for the green and efficient development of *in-situ* leaching mining.

Data availability statement

The original contributions presented in the study are included in the article/supplementary material, further inquiries can be directed to the corresponding authors.

Author contributions

J-LT: Conceptualization, Data curation, Formal Analysis, Funding acquisition, Investigation, Methodology, Project administration, Writing–original draft. Y-CD: Formal Analysis, Investigation, Methodology, Software, Writing–review and editing. D-XY: Data curation, Formal Analysis, Investigation, Methodology, Software, Writing–review and editing. B-FC: Data curation, Investigation, Methodology, Resources, Software, Writing–review and editing. YZ: Data curation, Formal Analysis, Investigation, Methodology, Writing–review and editing. J-GZ: Data curation, Formal Analysis, Methodology, Software, Writing–review and editing. XW: Data curation, Formal Analysis, Methodology, Writing–review and editing. WW: Conceptualization, Formal Analysis, Funding acquisition, Supervision, Validation, Writing–original draft.

Funding

Acknowledgments

Conflict of interest

The authors declare that the research was conducted in the absence of any commercial or financial relationships that could be construed as a potential conflict of interest.

Publisher's note

All claims expressed in this article are solely those of the authors and do not necessarily represent those of their affiliated organizations, or those of the publisher, the editors and the reviewers. Any product that may be evaluated in this article, or claim that may be made by its manufacturer, is not guaranteed or endorsed by the publisher.

References

Anikiev, D., Birnie, C., bin Waheed, U., Alkhalifah, T., Gu, C., Verschuur, D. J., et al. (2023). Machine learning in microseismic monitoring. *Earth-Science Rev.* 239, 104371. doi:10.1016/j.earscirev.2023.104371

Asadollahzadeh, M., Torkaman, R., and Torab-Mostaedi, M. (2021). Extraction and separation of rare earth elements by adsorption approaches: current status and future trends. *Sep. and Purif. Rev.* 50 (4), 417–444. doi:10.1080/15422119.2020.1792930

Azizi, M., Faz, A., Zornoza, R., Martínez-Martínez, S., Shahrokh, V., and Acosta, J. (2022). Environmental pollution and depth distribution of metal (loid) s and rare earth elements in mine tailing. *J. Environ. Chem. Eng.* 10 (3), 107526. doi:10.1016/j.jece.2022.107526

Balaram, V. (2019). Rare earth elements: a review of applications, occurrence, exploration, analysis, recycling, and environmental impact. *Geosci. Front.* 10 (4), 1285–1303. doi:10.1016/j.gsf.2018.12.005

Basta, F. F., Maurice, A. E., Fontboté, L., and Favarger, P.-Y. (2011). Petrology and geochemistry of the banded iron formation (BIF) of wadi karim and um anab, eastern desert, Egypt: implications for the origin of neoproterozoic BIF. *Precambrian Res.* 187 (3), 277–292. doi:10.1016/j.precamres.2011.03.011

Bharti, A. K., Prakash, A., Verma, A., and Singh, K. (2021). Assessment of hydrological condition in strata associated with old mine working during and post-monsoon using electrical resistivity tomography: a case study. *Bull. Eng. Geol. Environ.* 80, 5159–5166. doi:10.1007/s10064-021-02208-3

Borst, A. M., Smith, M. P., Finch, A. A., Estrade, G., Villanova-de-Benavent, C., Nason, P., et al. (2020). Adsorption of rare earth elements in regolith-hosted clay deposits. *Nat. Commun.* 11 (1), 4386. doi:10.1038/s41467-020-17801-5

Bustillo Revuelta, M. (2018). "Mineral resource exploration," in *Mineral resources: from exploration to sustainability assessment*, 121–222.

Chen, J. J., Liu, B., Wang, P. L., Yin, K., Li, Y., and He, P. (2018). Application research of integrated geophysical exploration techniques to gypsum mine gob. *Prog. Geophys.* 33 (2), 783–796. doi:10.6038/pg2018BB0086

Chen, S., Min, G., Liu, K., and Yuan, H. L. (2020). *Comparative study on the effect of 2D and 3D high-density electrical explorationan example of deep seepage channel investigation in a rare earth mining area[C]*. Chongqing: Annual meeting of Chinese geoscience union.

Chen, Z., Li, Z., Chen, J., Kallem, P., Banat, F., and Qiu, H. (2022). Recent advances in selective separation technologies of rare earth elements: a review. *J. Environ. Chem. Eng.* 10 (1), 107104. doi:10.1016/j.jece.2021.107104

Chen, Z. H. (2011). Global rare earth resources and scenarios of future rare earth industry. *J. rare earths* 29 (1), 1–6. doi:10.1016/s1002-0721(10)60401-2

Cheng, G., Ban, Y., Deng, X., Li, H., Zhang, H., Li, G., et al. (2023). Research on quantitative inversion of ion adsorption type rare earth ore based on convolutional neural network. *Front. Earth Sci.* 10, 1086325. doi:10.3389/feart.2022.1086325

Chi, R., and Liu, X. (2019). Prospect and development of weathered crust elution-deposited rare earth ore. *J. Chin. Soc. Rare Earths* 37 (2), 129–140. doi:10.11785/S1000-4343.20190201

Costa, N., Botelho, N., and Garnier, J. (2020). Concentration of rare earth elements in the Faixa Placha tin deposit, Pedra Branca A-Type Granitic Massif, central Brazil, and its potential for ion-adsorption-type REE-Y mineralization. *Ore Geol. Rev.* 123, 103606. doi:10.1016/j.oregeorev.2020.103606

Costis, S., Mueller, K. K., Coudert, L., Neculita, C. M., Reynier, N., and Blais, J.-F. (2021). Recovery potential of rare earth elements from mining and industrial residues: a review and cases studies. *J. Geochem. Explor.* 221, 106699. doi:10.1016/j.gexplo.2020.106699

Dushyantha, N., Batapola, N., Ilankoon, I., Rohitha, S., Premasiri, R., Abeysinghe, B., et al. (2020). The story of rare earth elements (REEs): occurrences, global distribution, genesis, geology, mineralogy and global production. *Ore Geol. Rev.* 122, 103521. doi:10.1016/j.oregeorev.2020.103521

Fan, C., Xu, C., Shi, A., Smith, M. P., Kynicky, J., and Wei, C. (2023). Origin of heavy rare earth elements in highly fractionated peraluminous granites. *Geochimica Cosmochimica Acta* 343, 371–383. doi:10.1016/j.gca.2022.12.019

Fu, W., Li, X., Feng, Y., Feng, M., Peng, Z., Yu, H., et al. (2019). Chemical weathering of S-type granite and formation of Rare Earth Element (REE)-rich regolith in South China: critical control of lithology. *Chem. Geol.* 520, 33–51. doi:10.1016/j.chemgeo.2019.05.006

Ghosh, G., and Sivakumar, C. (2018). Application of underground microseismic monitoring for ground failure and secure longwall coal mining operation: a case study in an Indian mine. *J. Appl. Geophys.* 150, 21–39. doi:10.1016/j.jappgeo.2018.01.004

Guo, Z., Jin, J., Zhao, K., Wang, X., and Chen, G. (2018). Status of leaching technology and theory of ion adsorption type rare earth ores. *Chin. Rare Earths* 39 (1), 132–141.

Guo, Z., Liu, L., Zhou, K., Wang, X., and Zhong, W. (2023). Research on the saturated/unsaturated seepage laws of ionic rare earth ore under different leaching conditions. *Front. Earth Sci.* 11, 1212017. doi:10.3389/feart.2023.1212017

Guo, Z., Zhao, K., Jin, J., Yuan, W., and Liang, C. (2019). Problems facing ion adsorption type rare earth exploitation and research progresses on green extraction. *Chem. Industry Eng. Prog.* 38 (7), 3425–3433. doi:10.16085/j.issn.1000-6613.2018-1687

He, Q., Qiu, J., Chen, J., Zan, M., and Xiao, Y. (2022). Progress in green and efficient enrichment of rare earth from leaching liquor of ion adsorption type rare earth ores. *J. Rare Earths* 40 (3), 353–364. doi:10.1016/j.jre.2021.09.011

Ibs-von Seht, M., and Wohlenberg, J. (1999). Microtremor measurements used to map thickness of soft sediments. *Bull. Seismol. Soc. Am.* 89 (1), 250–259. doi:10.1785/bssa0890010250

Ji, Y. H., Gao, Y., Chen, J. L., Yang, Z. C., Zhang, Z. C., Li, H., et al. (2021). Research progress on anticancer drugs of rare earth complexes. *J. Chin. Soc. Rare Earths* 39 (1), 197–205. doi:10.11785/S1000-4343.20210201

Jia, X., Sun, J. W., Liu, X. D., Chen, X. D., and Huang, H. L. (2022). Application of microtremor survey and high density electrical method in exploration of small-scale old goaf. *Geol. Surv. China* 9 (6), 42–50. doi:10.19388/j.zgdzdc.2022.06.06

Kanazawa, Y., and Kamitani, M. (2006). Rare earth minerals and resources in the world. *J. alloys Compd.* 408, 1339–1343. doi:10.1016/j.jallcom.2005.04.033

Li, H., Xu, F., and Weng, X. (2020). Recognition method for high-resolution remote-sensing imageries of ionic rare earth mining based on object-oriented technology. *Arabian J. Geosciences* 13, 1137–1147. doi:10.1007/s12517-020-06104-0

Li, M. Y. H., Kwong, H. T., Williams-Jones, A. E., and Zhou, M.-F. (2022). The thermodynamics of rare earth element liberation, mobilization and supergene enrichment during groundwater-regolith interaction. *Geochimica Cosmochimica Acta* 330, 258–277. doi:10.1016/j.gca.2021.05.002

Li, M. Y. H., and Zhou, M.-F. (2020). The role of clay minerals in formation of the regolith-hosted heavy rare earth element deposits. *Am. Mineralogist* 105 (1), 92–108. doi:10.2138/am-2020-7061

Li, M. Y. H., Zhou, M.-F., and Williams-Jones, A. E. (2019). The genesis of regolith-hosted heavy rare earth element deposits: insights from the world-class Zudong deposit in Jiangxi Province, South China. *Econ. Geol.* 114 (3), 541–568. doi:10.5382/econgeo.4642

Liu, W.-S., Wu, L.-L., Zheng, M.-Y., Chao, Y.-Q., Zhao, C.-M., Zhong, X., et al. (2019). Controls on rare-earth element transport in a river impacted by ion-adsorption rare-earth mining. *Sci. Total Environ.* 660, 697–704. doi:10.1016/j.scitotenv.2019.01.076

Liu, X.-R., Liu, W.-S., Tang, Y.-T., Wang, S.-Z., Cao, Y.-J., Chen, Z.-W., et al. (2022). Effects of in situ leaching on the origin and migration of rare earth elements in aqueous systems of South China: insights based on REE patterns, and Ce and Eu anomalies. *J. Hazard. Mater.* 435, 128959. doi:10.1016/j.jhazmat.2022.128959

Luo, F., Yan, J. Y., Liang, J., Zhang, S., Wu, D. H., Rao, G. W., et al. (2024). Application status and prospect of geophysical technology in rare-earth resources field. *J. Chin. Soc. rare earths* 06, 1088–1101. doi:10.12345/smg.v6i5.21056

Meng, X., Zhao, H., Zhao, Y., Shen, L., Gu, G., and Qiu, G. (2023). Heap leaching of ion adsorption rare earth ores and REEs recovery from leachate with lixiviant regeneration. *Sci. Total Environ.* 898, 165417. doi:10.1016/j.scitotenv.2023.165417

Moldoveanu, G., and Papangelakis, V. (2016). An overview of rare-earth recovery by ion-exchange leaching from ion-adsorption clays of various origins. *Mineral. Mag.* 80 (1), 63–76. doi:10.1180/minmag.2016.080.051

Ram, R., Becker, M., Brugger, J., Etschmann, B., Burcher-Jones, C., Howard, D., et al. (2019). Characterisation of a rare earth element-and zirconium-bearing ion-adsorption clay deposit in Madagascar. *Chem. Geol.* 522, 93–107. doi:10.1016/j.chemgeo.2019.05.011

Sanematsu, K., and Watanabe, Y. (2016). Characteristics and genesis of ion adsorption-type rare earth element deposits. *Soc. Econ. Geol.* 18. doi:10.5382/Rev.18.03

Simiyu, S. M. (2009). "Application of micro-seismic methods to geothermal exploration: examples from the Kenya Rift," in Proceedings of the Short Course VIII on Exploration for Geothermal Resources (Lake Naivasha, Kenya: United Nations University Geothermal Training Programme).31.

Sinclair, L., and Thompson, J. (2015). *In situ leaching of copper: challenges and future prospects. Hydrometallurgy* 157, 306–324. doi:10.1016/j.hydromet.2015.08.022

Smith, N. R. A., Reading, A. M., Asten, M. W., and Funk, C. W. (2013). Constraining depth to basement for mineral exploration using microtremor: a demonstration study from remote inland Australia. *Geophysics* 78 (5), B227–B242. doi:10.1190/geo2012-0449.1

Sobri, N., Yunus, M., and Harun, N. (2023). A review of ion adsorption clay as a high potential source of rare earth minerals in Malaysia. *Mater. Today Proc.* doi:10.1016/j.matpr.2023.03.513

Sobri, N. A. M., Harun, N., and Yunus, M. Y. M. (2024). A review of the ion exchange leaching method for extracting rare earth elements from ion adsorption clay. *Chem. Eng. Res. Des.* 208, 94–114. doi:10.1016/j.cherd.2024.06.023

Sun, Y. J., Xu, P. F., Ling, S. Q., and Li, C. J. (2009). Microtremor survey method and its progress. *Prog. Geophys* 24 (1), 326–334. doi:10.1190/1.9781560801740

Tian, J., Yin, J. Q., Chi, R., Rao, G. H., Jiang, M. T., and Ouyang, K. X. (2010). Kinetics on leaching rare earth from the weathered crust elution-deposited rare earth ores with ammonium sulfate solution. *Hydrometallurgy* 101 (3-4), 166–170. doi:10.1016/j.hydromet.2010.01.001

Traore, M., Gong, A., Wang, Y., Qiu, L., Bai, Y., Zhao, W., et al. (2023). Research progress of rare earth separation methods and technologies. *J. Rare Earths* 41 (2), 182–189. doi:10.1016/j.jre.2022.04.009

Wall, F. (2014). "Rare earth elements," in *Critical metals handbook*, 312–339.

Wang, D., Zhao, Z., Yu, Y., Wang, C., Dai, J., Sun, Y., et al. (2017). A review of the achievements in the survey and study of ion-absorption type REE deposits in China. *Acta Geosci. Sin.* 38 (3), 317–325. doi:10.3975/cagsb.2017.03.02

Wang, L., Wang, C., Li, L., and Yang, Y.-M. (2018a). Readsorption of rare earth elements during leaching process of ion-adsorption-type rare earth ore. *Rare Met.* 42 (6), 2113–2120. doi:10.1007/s12598-018-1162-3

Wang, W., Zeng, M.-F., Zhou, M.-F., Zhao, J.-H., Zheng, J.-P., and Lan, Z.-F. (2018b). Age, provenance and tectonic setting of Neoproterozoic to early Paleozoic sequences in southeastern South China Block: constraints on its linkage to western Australia-East Antarctica. *Precambrian Res.* 309, 290–308. doi:10.1016/j.precamres.2017.03.002

Wang, Z. W., Li, X. B., Zhao, D. P., Shang, X. Y., and Dong, L. J. (2018c). Time-lapse seismic tomography of an underground mining zone. *Int. J. Rock Mech. Min. Sci.* 107, 136–149. doi:10.1016/j.ijrmms.2018.04.038

Xiao, Y. F., Li, H., Long, Z. Q., Feng, Z. Y., and Wang, L. S. (2016). Adsorption ability of rare earth elements on clay minerals and its practical performance. *J. Rare Earths* 34 (5), 543–548. doi:10.1016/j.s1002-0721(16)60060-1

Xue, E. K., Chew, D., Drakou, F., and Wang, W. (2024). Detrital multi-mineral provenance constraints on the reconstruction of the South China Block within Gondwana. *Earth-Science Rev.* 253, 104798. doi:10.1016/j.earscirev.2024.104798

Xue, E. K., Wang, W., Huang, S.-F., and Lu, G.-M. (2019). Detrital zircon U-Pb-Hf isotopes and whole-rock geochemistry of neoproterozoic-cambrian successions in the Cathaysia Block of South China: implications on paleogeographic reconstruction in supercontinent. *Precambrian Res.* 331, 105348. doi:10.1016/j.precamres.2019.105348

Xue, E. K., Wang, W., Zhou, M. F., Pandit, M. K., Huang, S. F., and Lu, G. M. (2021). Late Neoproterozoic–early Paleozoic basin evolution in the Cathaysia Block, South China: implications of spatio-temporal provenance changes on the paleogeographic reconstructions in supercontinent cycles. *Geol. Soc. Am. Bull.* 133 (3-4), 717–739. doi:10.1130/b35588.1

Yang, X. J., Lin, A. J., Li, X. L., Wu, Y. D., Zhou, W. B., and Chen, Z. H. (2013). China's ion-adsorption rare earth resources, mining consequences and preservation. *Environ. Dev.* 8, 131–136. doi:10.1016/j.envdev.2013.03.006

Yang, Z. L., and Guo, K. (2020). The application of high density electrical method in detection of concealed goaf in iron mine. *China Min. Mag.* 29 (8), 158–164. doi:10.12075/j.issn.1004-4051.2020.08.008

Yaraghi, A., Ariffin, K., and Baharun, N. (2019). A short review on REE recovery from ion-adsorption clays. *Development* 8, 131–136. doi:10.31031/AMMS.2019.02.000550

Zhao, B., She, Z., and Kang, Q. (2017). Applicability evaluation and classification of insitu leaching mining for ion-absorbed-type rare earth deposit. *Min. Metallurgical Eng.* 37 (3), 6–10. doi:10.16533/J.CNKI.15-1099/TF.201904004

Zhao, L., Zhai, M., and Zhou, X. (2022). Formation of an intracontinental orogen above the permo-triassic mantle convection cell in the paleo-tethys tectonic realm due to far-field stress derived from continental margins. *Front. Earth Sci.* 10, 892787. doi:10.3389/feart.2022.892787

Zhao, Z., Wang, D.-h., Chen, Z.-y., Chen, Z., Zheng, G., and Liu, X. (2014). Zircon U-Pb age, endogenic mineralization and petrogenesis of rare earth ore-bearing granite in Longnan, Jiangxi Province. *Acta Geosci. Sin.* 35 (6), 719–725. doi:10.3975/cagsb.2014.06.07

Zhong, J. G., Ye, D. X., Wu, Y. G., Chen, B. F., Deng, Y. C., and Qi, F. Y. (2022). Integrated application of High-density electrical measurement and drilling data in ion-adsorption type rare earth mines. *Chin. Rare Earths* 43 (1), 82–91. doi:10.16533/J.CNKI.15-1099/TF.20230005

Zhou, J., Wang, X., Nie, L., McKinley, J. M., Liu, H., Zhang, B., et al. (2020). Geochemical background and dispersion pattern of the world's largest REE deposit of Bayan Obo, China. *J. Geochem. Explor.* 215, 106545. doi:10.1016/j.gexplo.2020.106545